

# Magnetosphere-Ionosphere Coupling by Alfvén Waves: Beyond Current Continuity

R. L. Lysak and Y. Song

*School of Physics and Astronomy, University of Minnesota, 116 Church Street SE, Minneapolis, MN 55455 USA*

## Abstract

Many numerical models of magnetospheric dynamics treat the ionosphere as an inner boundary condition. These models have traditionally used the current continuity condition, treating the ionosphere as a sheet current in which the electric field is electrostatic. A more general boundary condition is suggested that not only is more complete, but also straightforward to implement. Results from a model using this boundary condition applied to the excitation of field line resonances in the magnetosphere are presented.

## 1. Introduction

Numerical modeling of the magnetosphere has proven to be a useful technique for the description of magnetospheric dynamics. Most such models on the global scale are based on the ideal MHD equations, using various numerical methods for their implementation (e.g., Fedder and Lyon, 1987; Fedder et al., 1998; Raeder et al., 1998, 2001; Groth et al., 2000; Slinker et al., 2001). The inner boundary condition of such models is generally at rather large distances from the Earth, for example,  $3.5 R_E$  radial distance in the Raeder et al. (2001) model. This large distance is dictated by the geometry of the magnetic field lines and the fact that the Alfvén speed becomes very large below this altitude. For example, the Alfvén speed is  $10^5$  km/s for a magnetic field of 0.05 G and a density of  $1 \text{ cm}^{-3}$ , typical parameters in the auroral acceleration region at about  $2 R_E$  radial distance. This large wave speed puts strong constraints on the time step that can be used, since the Courant stability condition states that the time step must be small enough that waves travel less than one grid point in a time step.

As a result, these global models simplify the inner boundary using an electrostatic condition for the ionosphere. The magnetic fields at this inner boundary will generally have a curl, corresponding to a field-aligned current according to Ampere’s Law. This current is assumed to propagate along field lines to the ionosphere, where it is closed by means of ionospheric currents. If the ionosphere is modeled as a thin slab, these currents can be represented by height-integrated conductances corresponding to the Pedersen and Hall conductivities of the ionosphere. Then, current continuity in the ionosphere leads to the relation

$$j_{\parallel} \cos \alpha = \nabla_h \cdot \vec{\Sigma} \cdot \nabla_h \Phi \quad (1)$$

Here the angle  $\alpha$  represents the angle between the vertical and the magnetic field direction (hence,  $\alpha < 90^\circ$  in the southern hemisphere and  $\alpha > 90^\circ$  in the northern hemisphere) and the subscript  $h$  emphasizes that the horizontal components of the gradient are being taken. This relation is then solved for the electrostatic potential  $\Phi$ , which is then mapped back up to the inner boundary of the simulation, where it is used as a velocity boundary condition by invoking the

$\mathbf{E} \times \mathbf{B}$  drift,  $\mathbf{v} = -\nabla\Phi \times \mathbf{B} / B^2$ . Note that various models can be used for the conductances, depending on solar zenith angle and precipitating energy fluxes (e.g., Raeder et al., 2001).

On the other hand, more local models of the interaction of the ionosphere with ULF waves indicate that this model is inadequate to describe fluctuations at small spatial scales and/or higher frequencies. For example, it has long been known that fluctuations in the Pc1 frequency range (0.2-5.0 Hz) can propagate in the so-called Pc1 waveguide (Greifinger and Greifinger, 1968, 1973; Fraser, 1975; Fujita and Tamao, 1988). These fluctuations propagate in the fast compressional mode, in which the electric field perturbations are not electrostatic. More recently, Yoshikawa and Itonaga (1996, 2000) investigated the properties of an inductive (i.e., non-electrostatic) ionosphere and showed that inductive effects can modify the reflection of shear mode Alfvén waves from the ionosphere, even at lower frequencies. In these models, the Hall conductivity plays the role of coupling the shear Alfvén wave and the fast compressional wave, which cannot be described using the electrostatic model. Sciffer and Waters (2002) and Sciffer et al. (2004) have considered this inductive model in the presence of dipole tilt, noting that the inductive effect is enhanced by a tilted dipole field.

Based on these considerations, Lysak (2004) has developed a three-dimensional numerical model including dipole tilt effects that uses a boundary condition that can take all of these effects into account. The purpose of this report is to focus on the ionospheric boundary condition in this model and describe its potential for inclusion in global models of magnetospheric dynamics.

## 2. Ionospheric Jump Conditions

A boundary condition for the ionosphere can be found by treating the current-carrying region of the ionosphere as a thin slab at a constant radial distance  $r$ , within which the current can be written as:

$$\mathbf{j} = \sigma_P \mathbf{E}_\perp - \sigma_H \mathbf{E} \times \hat{\mathbf{b}} + \sigma_0 E_\parallel \hat{\mathbf{b}} \quad (2)$$

Note that here  $\hat{\mathbf{b}}$  is a unit vector in the direction of the background magnetic field, which can be in any direction with respect to the radial direction  $\hat{\mathbf{r}}$ . With these definitions, the angle  $\alpha$  given in Eq. (1) can be written as  $\cos \alpha = \hat{\mathbf{b}} \cdot \hat{\mathbf{r}}$ . Note also that the minus sign in the Hall term is included so that the Hall conductivity is positive when the electrons carry the Hall current. If we then integrate Eq. (2) over the thickness of the ionosphere, we can write the height-integrated current as (e.g., Sciffer and Waters, 2002)

$$\mathbf{I} = \vec{\Sigma} \cdot \mathbf{E} = \begin{pmatrix} \frac{\Sigma_0 \Sigma_P}{\Sigma_{zz}} & -\frac{\Sigma_0 \Sigma_H \cos \alpha}{\Sigma_{zz}} \\ \frac{\Sigma_0 \Sigma_H \cos \alpha}{\Sigma_{zz}} & \Sigma_P + \frac{\Sigma_H^2 \sin^2 \alpha}{\Sigma_{zz}} \end{pmatrix} \begin{pmatrix} E_\theta \\ E_\varphi \end{pmatrix} \quad (3)$$

Here  $E_\theta$  and  $E_\varphi$  are the horizontal spherical components of the electric field, which are assumed to be constant across the slab, and it has been assumed that the radial component of the current vanishes. In this equation,  $\Sigma_0$ ,  $\Sigma_P$ , and  $\Sigma_H$  are the height-integrated parallel, Pedersen, and Hall conductivities, respectively, and we define  $\Sigma_{zz} = \Sigma_0 \cos^2 \alpha + \Sigma_P \sin^2 \alpha$ , which enters the conductivity tensor due to the condition that the radial current in the slab vanishes. Note that the parallel conductance  $\Sigma_0$  is usually orders of magnitude greater than the perpendicular conductances, and making this assumption the conductivity tensor can be written

$$\vec{\Sigma} = \begin{pmatrix} \frac{\Sigma_P}{\cos^2 \alpha} & -\frac{\Sigma_H}{\cos \alpha} \\ \frac{\Sigma_H}{\cos \alpha} & \Sigma_P \end{pmatrix} \quad (4)$$

Note that these forms are valid in both hemispheres; since  $\cos \alpha$  changes sign across the equator, the off-diagonal terms also change sign.

The boundary condition for electric and magnetic fields can be given by the usual electromagnetic jump conditions (e.g., Jackson, 1999):

$$\mu_0 \mathbf{I} = \hat{\mathbf{r}} \times \Delta \mathbf{B} \quad \hat{\mathbf{r}} \cdot \Delta \mathbf{B} = 0 \quad \hat{\mathbf{r}} \times \Delta \mathbf{E} = 0 \quad (5)$$

In these relations the  $\Delta$  denotes the change of the variable above and below the slab, e.g.,  $\Delta \mathbf{B} = \mathbf{B}_{above} - \mathbf{B}_{below}$ . Note that the last of these conditions states that the horizontal electric field is continuous across the slab, as assumed in the derivation of Eq. (3). It may be noted that the standard current continuity condition Eq. (1) can be found by taking the horizontal divergence of the first relation in Eq. (5):

$$\mu_0 \nabla_h \cdot (\vec{\Sigma} \cdot \mathbf{E}) = \nabla_h \cdot (\hat{\mathbf{r}} \times \Delta \mathbf{B}) = -\hat{\mathbf{r}} \cdot (\nabla_h \times \Delta \mathbf{B}) = -\mu_0 j_r \quad (6)$$

In the last step of this expression it has been assumed that the atmosphere (the region below the ionospheric slab) is a perfect insulator, implying that no current can flow in this region. Note that writing  $j_r = j_{||} \cos \alpha$  and assuming an electrostatic ionosphere,  $\mathbf{E} = -\nabla \Phi$  leads to Eq. (1).

However, the boundary conditions given by (5) are more general than Eq. (1). In particular, we can take the radial component of the curl of Eq. (5) to yield a new condition

$$\mu_0 \hat{\mathbf{r}} \cdot [\nabla \times (\vec{\Sigma} \cdot \mathbf{E})] = \hat{\mathbf{r}} \cdot [\nabla \times (\hat{\mathbf{r}} \times \Delta \mathbf{B})] = \nabla_h \cdot \Delta \mathbf{B} = -\Delta (\partial B_r / \partial r) \quad (7)$$

Here in the last step we have used the divergence-free condition,  $\nabla \cdot \mathbf{B} = 0$ , and we note that while the radial component of  $\mathbf{B}$  does not change across the slab according to the second relation in Eq. (5), the derivative of this component can in fact change (In general,  $B_r$  as a function of  $r$  would have a cusp-like behavior across the slab). The physical significance of Eq. (6) and (7) can be most easily seen by considering the case of a vertical background field and assuming a uniform conductivity, in which case these equations become

$$\begin{aligned} \Sigma_P \nabla_{\perp} \cdot \mathbf{E}_{\perp} - \Sigma_H \hat{\mathbf{r}} \cdot (\nabla \times \mathbf{E}_{\perp}) &= -j_{||} \\ \Sigma_H \nabla_{\perp} \cdot \mathbf{E}_{\perp} + \Sigma_P \hat{\mathbf{r}} \cdot (\nabla \times \mathbf{E}_{\perp}) &= (1/\mu_0) \Delta (\partial B_r / \partial r) \end{aligned} \quad (8)$$

Thus, these equations decouple when the Hall conductivity vanishes, with the first equation giving the current closure due to the shear Alfvén wave and the second equation describes the fast compressional wave. Note that in the absence of the inductive (i.e.,  $\nabla \times \mathbf{E}_{\perp}$ ) term, the first condition gives the usual current continuity while the second condition relates to the production of the ground signature of the wave (see next section).

Note that to be useful as a boundary condition, Eq. (5) requires knowledge of the magnetic fields above and below the ionosphere. The fields above the ionosphere would be supplied by the magnetospheric simulation; however, that simulation would not have knowledge of the fields below the ionosphere. Finding an atmospheric solution is the subject of the next section.

### 3. The atmospheric solution

To find the magnetic fields in the atmosphere, we must note the conditions that prevail in this region. First of all, the atmosphere is assumed to be perfectly insulating, i.e., no currents can flow in this region. Therefore, the curl of the magnetic field must be zero. As is well known from the theory of electromagnetism, a curl-free field can be written as the gradient of a scalar, e.g.,  $\delta\mathbf{B} = \nabla\Psi$ , where  $\Psi$  is referred to as the magnetic scalar potential. Note that here we are considering just perturbations of the magnetic field; the background geomagnetic field can be superposed on this solution. Furthermore, since the magnetic field is always divergence free,  $\nabla \cdot \delta\mathbf{B} = \nabla^2\Psi = 0$ ; thus, the magnetic scalar potential satisfies Laplace's equation, and can thus be solved if appropriate boundary conditions are taken. At the ground, the Earth can be considered to be a perfect conductor to lowest approximation; thus, the electric fields are zero and the magnetic field can be considered to be frozen-in to the Earth. Thus, the vertical component of the magnetic field must vanish at the ground, or  $\delta B_r = \partial\Psi / \partial r = 0$ .

At the top of the atmosphere, the ionosphere, we can take a boundary condition from the second relation of Eq. (5), i.e., the radial component of the magnetic field perturbation at the ionosphere is given, since it is continuous with the corresponding component above the ionosphere. Taking  $r = R_E$  to be the radius of the Earth and  $r = R_I$  to be the ionosphere, we therefore have the boundary conditions

$$\left. \frac{\partial\Psi}{\partial r} \right|_{r=R_E} = 0 \quad \left. \frac{\partial\Psi}{\partial r} \right|_{r=R_I} = B_{rI} \quad (9)$$

where  $B_{rI}$  is the radial component of the ionospheric magnetic field.

It is instructive to first consider this relation in a slab geometry, where we will take the ground to be  $z = 0$  and the ionosphere to be  $z = H$ . Let the ionospheric radial field be a sinusoidal wave,  $B_{zI} = B_{z0}e^{ik_{\perp}x}$ . Assuming  $\Psi$  also has this perpendicular variation, Laplace's equation can be written as

$$\frac{\partial^2\Psi}{\partial z^2} - k_{\perp}^2\Psi = 0 \quad (10)$$

which has solutions  $\Psi = A \cosh k_{\perp}z + B \sinh k_{\perp}z$ . Applying the boundary condition at the ground implies that  $B = 0$ , and applying the ionospheric condition gives the solution

$$\Psi = \frac{B_{zI}}{k_{\perp}} \frac{\cosh k_{\perp}z}{\sinh k_{\perp}H} e^{ik_{\perp}x} \quad (11)$$

Note that in the short wavelength limit,  $k_{\perp}H \gg 1$ , this solution is exponentially decreasing from the ionosphere as  $\exp[k_{\perp}(z-H)]$ .

The solution becomes more complex when considering the spherical geometry of the Earth. In the general case, it is desired to model the ionosphere between two latitudes,  $\theta_0 < \theta < \theta_1$ . For a perturbation that has an azimuthal dependence of  $\exp im\phi$ , the latitudinal part of Laplace's equation takes the form of Legendre's equation

$$\frac{d}{dx} \left[ (1-x^2) \frac{dP}{dx} \right] + \left[ v(v+1) - \frac{m^2}{1-x^2} \right] P = 0 \quad (12)$$

where  $x = \cos \theta$ . The solutions to this equation are the associated Legendre functions of the first and second kinds,  $P_v^m(x)$  and  $Q_v^m(x)$ . Applying boundary conditions at the bounding latitudes (either Dirichlet or Neumann conditions may be used), the general solution for Laplace's equation takes the form

$$\Psi(r, x, \varphi) = \sum_{l,m} \left( A_{lm} r^{v_{lm}} + B_{lm} r^{-(v_{lm}+1)} \right) y_{lm}(x, \varphi) \quad (13)$$

where we define a modified spherical harmonic as

$$y_{lm}(x, \varphi) = \left[ C_{lm} P_{v_{lm}}^m(x) + D_{lm} Q_{v_{lm}}^m(x) \right] e^{im\varphi} \quad (14)$$

Note here  $l$  is an integer that denotes the mode number, not the degree of the Legendre functions. The degree of the Legendre functions  $v_{lm}$  and the ratio  $D_{lm} / C_{lm}$  are determined from the boundary conditions, with the constant  $C_{lm}$  being determined by the normalization condition. In practice, it is difficult to generate these functions for non-integer degree, and so Eq. (12) is integrated numerically and the degree  $v_{lm}$  is determined by a root finding method. Figure 1 shows the first 5 solutions to Eq. (12) for  $m = 2$  and  $m = 10$  for a run in which Dirichlet boundary conditions were applied at latitudes of  $54.2^\circ$  and  $71.4^\circ$  (roughly  $L = 3$  and  $L = 10$  field lines).

Once these eigenfunctions are obtained, they can be used in Eq. (13) to get a full solution. The boundary condition at the ground,  $\partial\Psi / \partial r = 0$ , leads to the condition

$$\frac{B_{lm}}{A_{lm}} = \frac{v_{lm}}{v_{lm} + 1} R_E^{2v_{lm}+1} \quad (15)$$

Similarly, the ionospheric boundary condition gives the other coefficient

$$A_{lm} = \frac{1}{v_{lm} R_I^{v_{lm}-1} \left[ 1 - (R_E / R_I)^{2v_{lm}+1} \right]} \int d\Omega B_r(R_I, \theta, \varphi) y_{lm}^*(\theta, \varphi) \quad (16)$$

In practice, these coefficients are found by least squares fit to the values of  $B_r$  at the ionosphere using singular value decomposition. It should be noted that the coefficients of this decomposition need only to be computed at the beginning of the simulation, and can then be used repeatedly during the simulation as the system evolves.

#### 4. Coupling to a numerical model

The boundary condition described above is suitable to be used in a wide range of numerical models that describe the dynamics of the magnetosphere. As one example, this boundary condition has been applied to a linear MHD wave model that uses non-orthogonal coordinates (Lysak, 2004). These coordinates are useful since the dynamics of the MHD equations suggests a magnetic-field-aligned coordinate system, while the structure of the ionosphere, as discussed above, suggests the usefulness of a spherical coordinate system. In non-orthogonal coordinates there is a distinction between contravariant and covariant basis vectors, with the contravariant basis vectors being perpendicular to the coordinate planes (i.e., the planes defined by one of the coordinates being constant), and thus also are called normal basis vectors, and the covariant basis vectors being parallel to the coordinate lines (the lines defined by two of the coordinates being constant), and being called tangent basis vectors (d'Haeseleer et al., 1991). For a coordinate system in which the magnetic field lines are defined by the first two coordinates being constant, the first two contravariant basis vectors are perpendicular to the magnetic field while the third covariant vector is parallel to the magnetic field. The third coordinate is constant in the ionosphere at constant radial distance; therefore the third contravariant coordinate is radial while the first two covariant coordinates are horizontal. The two coordinate systems are related by the metric tensor, which essentially provides the rotation from one set of coordinates to another.

Thus in this code, the boundary condition is implemented as follows. The simulated fields are rotated into their spherical components. These components of the magnetic field can then be

used in the boundary conditions given by Eq. (5). Noting that the radial component of the magnetic field is continuous across the ionospheric layer, it can be used as a boundary condition for the atmospheric solution given by Eq. (16). This solution then gives the horizontal components of the magnetic field below the ionosphere. Then the first formula in Eq. (5) can be solved for the current in the ionosphere, and the ionospheric Ohm's law, Eq. (3) can be inverted to give the electric field in the ionosphere (which is continuous as seen by the third formula in Eq. (5)). A similar procedure could be used in any numerical model, provided appropriate mappings from the inner boundary of the model to the spherical components of the fields at the ionosphere are developed.

As an example of such a run, we consider a case in which a field line resonance has been excited with a compressional wave at the magnetopause. Parameters for such a run have been taken from the observations of Ponomarenko et al. (2004), who observed a 40-second period field line resonance with radar and ground observations near  $65^\circ$  south geomagnetic latitude. A compressional pulse with a width of 1000 km in longitude (mapped to the ionosphere) and centered at  $90^\circ$  longitude is introduced (note that longitude is arbitrary in this model, which assumes cylindrical symmetry.) The height-integrated Pedersen conductivity was 4 mho in this run, and the Hall conductance was 10 mho. Figure 2a shows a gray scale plot of the poleward electric field component in this run, with darker shades indicating negative values and lighter shades positive values. Figure 2b shows a cut at  $r = 2 R_E$  through this figure, giving a more quantitative view. It can be seen that enhancements occur at approximately  $65.4^\circ$  and  $68.0^\circ$  latitude. The 40-second driver wave corresponds to the 3<sup>rd</sup> and 5<sup>th</sup> harmonics on these resonant field lines. Figure 3 shows the electric and magnetic field profiles along these field lines, demonstrating the 3<sup>rd</sup> and 5<sup>th</sup> harmonic structure of the wave (note that only half the field line is shown).

Figure 4 shows a comparison of magnetic fields above and below the ionosphere. Figure 4a shows a vector plot of the perpendicular components of the magnetic field at 600 km altitude, while Figure 4b shows the corresponding plots of the ground magnetic field. It can be seen that the ground fields are rotated by  $90^\circ$  from the fields above the ionosphere, as expected, and that the smaller scale structures in the magnetic field are smoothed out in the ground signature. For another view of the ground signature, Figure 5 shows stacked plots of the time history of the latitudinal component of the magnetic field from 4 points at  $120^\circ$  longitude on L-shells of 4.5, 5.6, 6.7, 7.8, and 9.0, corresponding to latitudes of  $61.9$ ,  $65.0$ ,  $67.3$ ,  $69.0$  and  $70.5$  degrees. Each curve is displaced upward by 20 nT, with the most poleward location on top. This figure clearly shows the poleward phase progression of the wave signal. A strong field line resonance signature is not so well seen however (note that the second and fourth of these curves from the top represent the 5<sup>th</sup> and 3<sup>rd</sup> harmonic field lines).

## 5. Conclusions

The calculations presented here show the usefulness of adopting a more general boundary condition for the ionosphere, based on the electromagnetic jump conditions across the boundary rather than on current continuity. This model gives the ground magnetic fields directly, rather than requiring a solution of the Biot-Savart Law as described Raeder et al. (2001). The traditional solution requires a solution of Poisson's equation with variable coefficients as described by Eq. (1). In this new model, Laplace's equation is solved with the compressional magnetic field as a boundary condition, which is generally simpler to solve. Note that while our

simple solution assumed a perfectly insulating atmosphere and a perfectly conducting ionosphere, these conditions can be relaxed without excessive difficulty (see, e.g., a two-dimensional solution with a finite atmospheric conductivity in Lysak, 1997).

While this model provides a more complete description of magnetosphere-ionosphere-atmosphere-ground coupling, it should be noted that the inductive effect is most important when dealing with long perpendicular wavelength and higher frequency (e.g., Yoshikawa et al., 1996, 2000). Thus, auroral zone models with short perpendicular wavelength and global models that consider only low frequency are described by the current continuity model to a reasonable accuracy. Dipole tilt effects, however, should certainly be included in such models, as is done in most global simulations using equations (1) and (4) (e.g., Raeder et al., 2001). In such models, however, the inner boundary is at  $3.5 R_E$ , or an invariant latitude of about  $58^\circ$ . This latitude corresponds to  $\cos \alpha = 0.980$ , so the tilt angle not too significant at such angles.

However, at lower latitudes, the work of Sciffer and Waters (2002) and Sciffer et al. (2004) shows that dipole tilt effects enhance the importance of the inductive term that is not included in the current continuity description. In addition, fields close to the ionospheric boundary, such as those measured by ionospheric radar, may be more strongly affected by this boundary condition. Waters (personal communication) has compared a version of his model with a fully resolved boundary condition to one with the boundary condition suggested here, and notes that the fields are indistinguishable except in the immediate vicinity of the boundary. Thus, while further work needs to be done to ascertain how important this generalized boundary condition is in practice, it is certainly no more difficult to implement and may give a better description of the ionospheric boundary for models of magnetospheric dynamics.

**Acknowledgements.** We would like to thank Colin Waters, Murray Sciffer, and Pasha Ponomarenko for useful discussions and suggestions on this model. This work was supported by NASA grant NAG5-13072 and NSF grant ATM-0201703. Computing services were provided by the Minnesota Supercomputer Institute. RLL would like to acknowledge the hospitality and support of the University of Newcastle, NSW, Australia, where part of this work was carried out.

## References

- D'Haeseleer, W. D., W. N. G. Hitchon, J. D. Callen, and J. L. Shohet, *Flux Coordinates and Magnetic Field Structure*, Springer-Verlag, Berlin, 1991.
- Fedder, J. A. and J. G. Lyon, The solar wind-magnetosphere-ionosphere current-voltage relationship, *Geophys. Res. Lett.*, *14*, 880, 1987.
- Fedder, J. A., S. P. Slinker, and J. G. Lyon, A comparison of global numerical simulation results to data for the January 27-28, 1992, Geospace Environment Modeling challenge event, *J. Geophys. Res.*, *103*, 14,799, 1998.
- Fraser, B. J., Ionospheric duct propagation and Pc1 pulsation source, *J. Geophys. Res.*, *80*, 2790, 1975.
- Fujita, S., and T. Tamao, Duct propagation of hydromagnetic waves in the upper ionosphere, 1, Electromagnetic field disturbances in high latitudes associated with localized incidence of a shear Alfvén wave, *J. Geophys. Res.*, *93*, 14,665, 1988.
- Greifinger, C., and P. Greifinger, Theory of hydromagnetic propagation in the ionospheric waveguide, *J. Geophys. Res.*, *73*, 7473, 1968.

- Greifinger, C., and P. Greifinger, Wave guide propagation of micropulsations out of the plane of the geomagnetic meridian, *J. Geophys. Res.*, *78*, 4611, 1973.
- Groth, C. P. T., D. L. DeZeeuw, T. I. Gombosi, and K. G. Powell, Global three-dimensional MHD simulation of a space weather event: CME formation, interplanetary propagation, and interaction with the magnetosphere, *J. Geophys. Res.*, *105*, 25,053, 2000.
- Jackson, J. D., *Classical Electrodynamics*, Third Edition, Wiley, New York, 1999.
- Lysak, R. L., Propagation of Alfvén waves through the ionosphere, *Phys. Chem. Earth*, *22*, 757, 1997.
- Lysak, R. L., Magnetosphere-ionosphere coupling by Alfvén waves at midlatitudes, *J. Geophys. Res.*, *109*, A07201, doi:10.1029/2004JA010454, 2004.
- Ponomarenko, P. V., F. W. Menk, C. L. Waters, and M. D. Sciffer, Pc3-4 ULF waves observed by the SuperDARN TIGER radar, submitted to *Ann. Geophys.*, 2004.
- Raeder, J., J. Berchem, and M. Ashour-Abdalla, The Geospace Environment Modeling grand challenge: Results from a global geospace circulation model, *J. Geophys. Res.*, *103*, 14,787, 1998.
- Raeder, J., R. L. McPherron, L. A. Frank, S. Kokubun, G. Lu, T. Mukai, W. R. Paterson, J. B. Sigwarth, H. J. Singer, and J. A. Slavin, Global simulation of the Geospace Environment Modeling substorm challenge event, *J. Geophys. Res.*, *106*, 381, 2001.
- Sciffer, M. D., and C. L. Waters, Propagation of ULF waves through the ionosphere: Analytic solutions for oblique magnetic fields, *J. Geophys. Res.*, *107*(A10), 1297, doi: 10.1029/2001JA000184, 2002.
- Sciffer, M. D., C. L. Waters, and F. W. Menk, Propagation of ULF waves through the ionosphere: Inductive effect for oblique magnetic fields, *Ann. Geophys.*, *22*, 1155, 2004.
- Slinker, S. P., J. A. Fedder, J. M. Ruohoniemi, and J. G. Lyon, Global MHD simulation of the magnetosphere for November 24, 1996, *J. Geophys. Res.*, *106*, 361, 2001.
- Yoshikawa, A., and M. Itonaga, Reflection of shear Alfvén waves at the inductive ionosphere, *Geophys. Res. Lett.*, *23*, 101, 1996.
- Yoshikawa, A., and M. Itonaga, The nature of reflection and mode conversion of MHD waves in the inductive ionosphere: Multistep mode conversion between divergent and rotational electric fields, *J. Geophys. Res.*, *105*, 10,565, 2000.

## Figure Captions

Figure 1. Plots of the first 5 eigenfunctions for Legendre's equation between the latitudes of  $54^\circ$  and  $71^\circ$  (roughly  $L=3$  and  $L=10$ ) with Dirichlet boundary conditions assumed at the boundaries. Top panel gives the eigenfunctions for  $m = 2$ , and the bottom panel for  $m = 10$ .

Figure 2. (a) Color plots of the poleward perpendicular component of the electric field at a longitude of  $60^\circ$  and time of 300 s into the run described in the text. Blue shades indicate negative values and green shades positive values. (b) Value of this component as a function of latitude at  $r = 2 R_E$  radial distance.

Figure 3. Plots of the (a) poleward perpendicular electric field and (b) eastward magnetic field components at the same time as the plot of Figure 2 at invariant latitudes of  $65.4^\circ$  (solid curves) and  $68.0^\circ$  (dotted curves), indicating 3<sup>rd</sup> and 5<sup>th</sup> harmonic structure, respectively.

Figure 4. Vector plots of the perpendicular magnetic field at (a) 600 km altitude and (b) the ground at the same time as the plots of Figures 2 and 3. Note the rotation of the magnetic field, the smoothing of the fine scale structure and the general reduction in magnitude from the ionosphere to the ground.

Figure 5. Stacked plots of the time history of the equatorward ground magnetic field at  $120^\circ$  longitude and L values of 4.5, 5.6, 6.7, 7.8, and 9.0, corresponding to latitudes of  $61.9$ ,  $65.0$ ,  $67.3$ ,  $69.0$  and  $70.5$  degrees, with the more poleward locations on the top. Note the general poleward phase progressions of the magnetic signals.

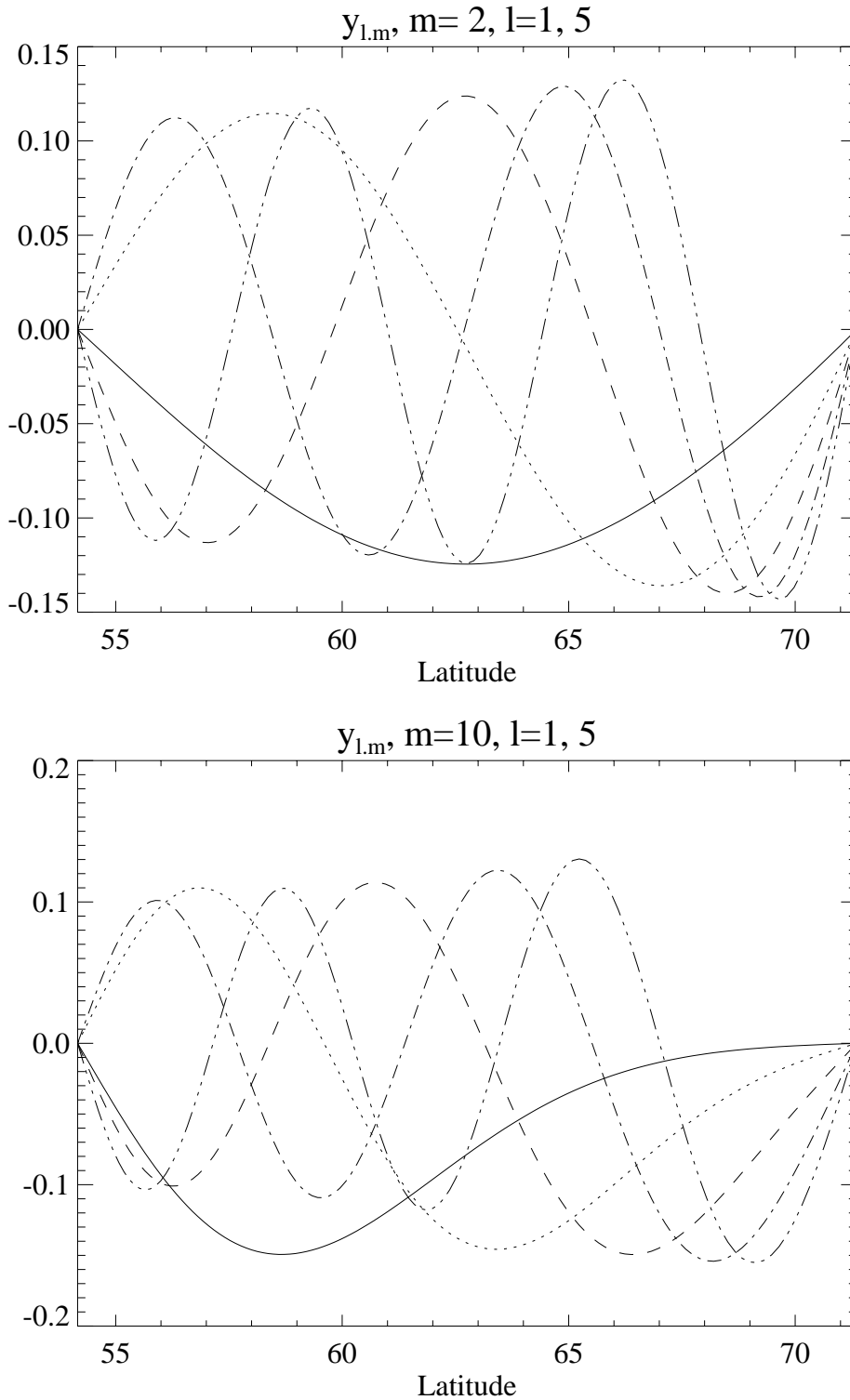


Figure 1. Plots of the first 5 eigenfunctions for Legendre's equation between the latitudes of  $54^\circ$  and  $71^\circ$  (roughly  $L=3$  and  $L=10$ ) with Dirichlet boundary conditions assumed at the boundaries. Top panel gives the eigenfunctions for  $m = 2$ , and the bottom panel for  $m = 10$ .

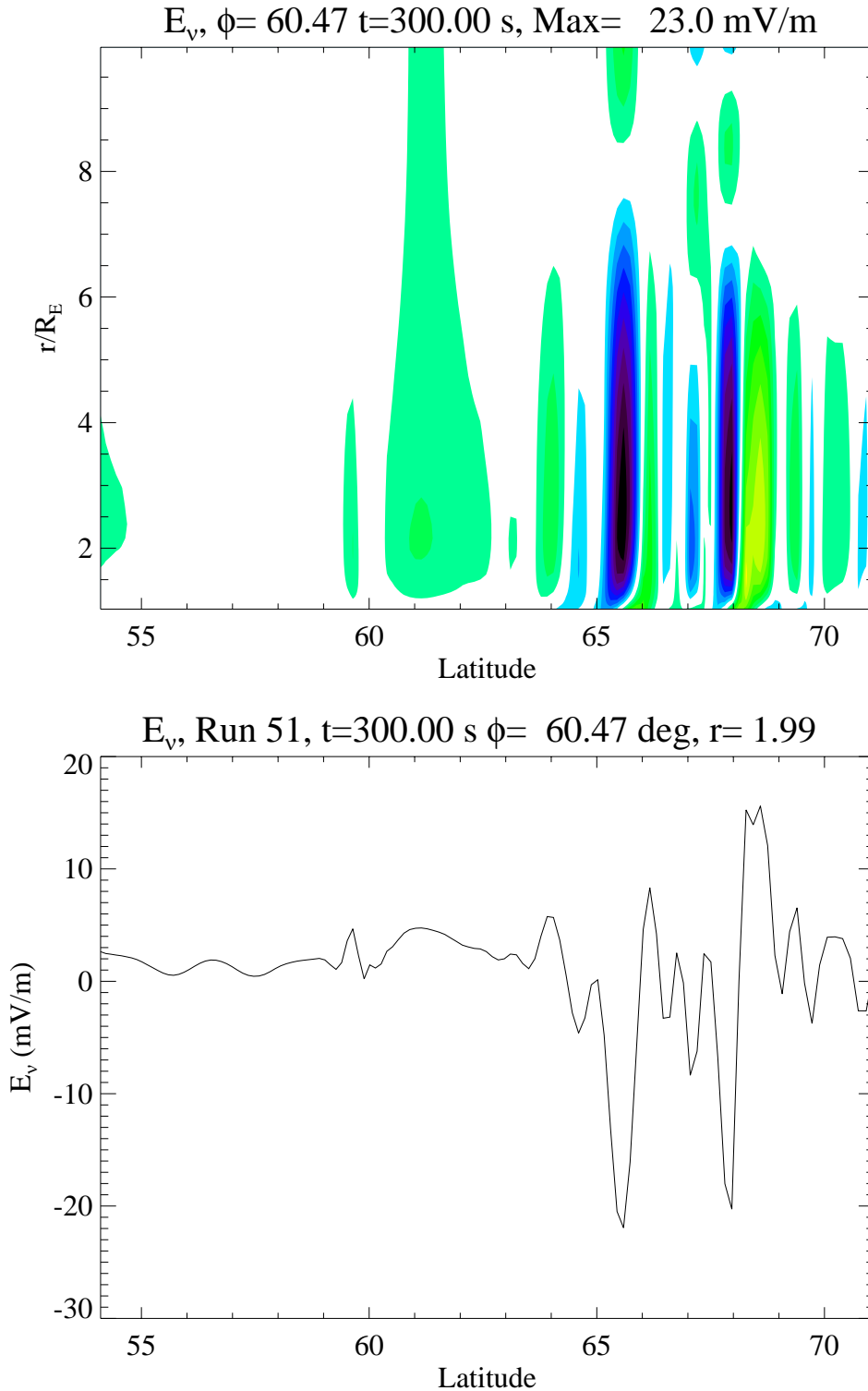


Figure 2. (a) Color plots of the poleward perpendicular component of the electric field at a longitude of  $60^\circ$  and time of 300 s into the run described in the text. Blue shades indicate negative values and green shades positive values. (b) Value of this component as a function of latitude at  $r = 2 R_E$  radial distance.

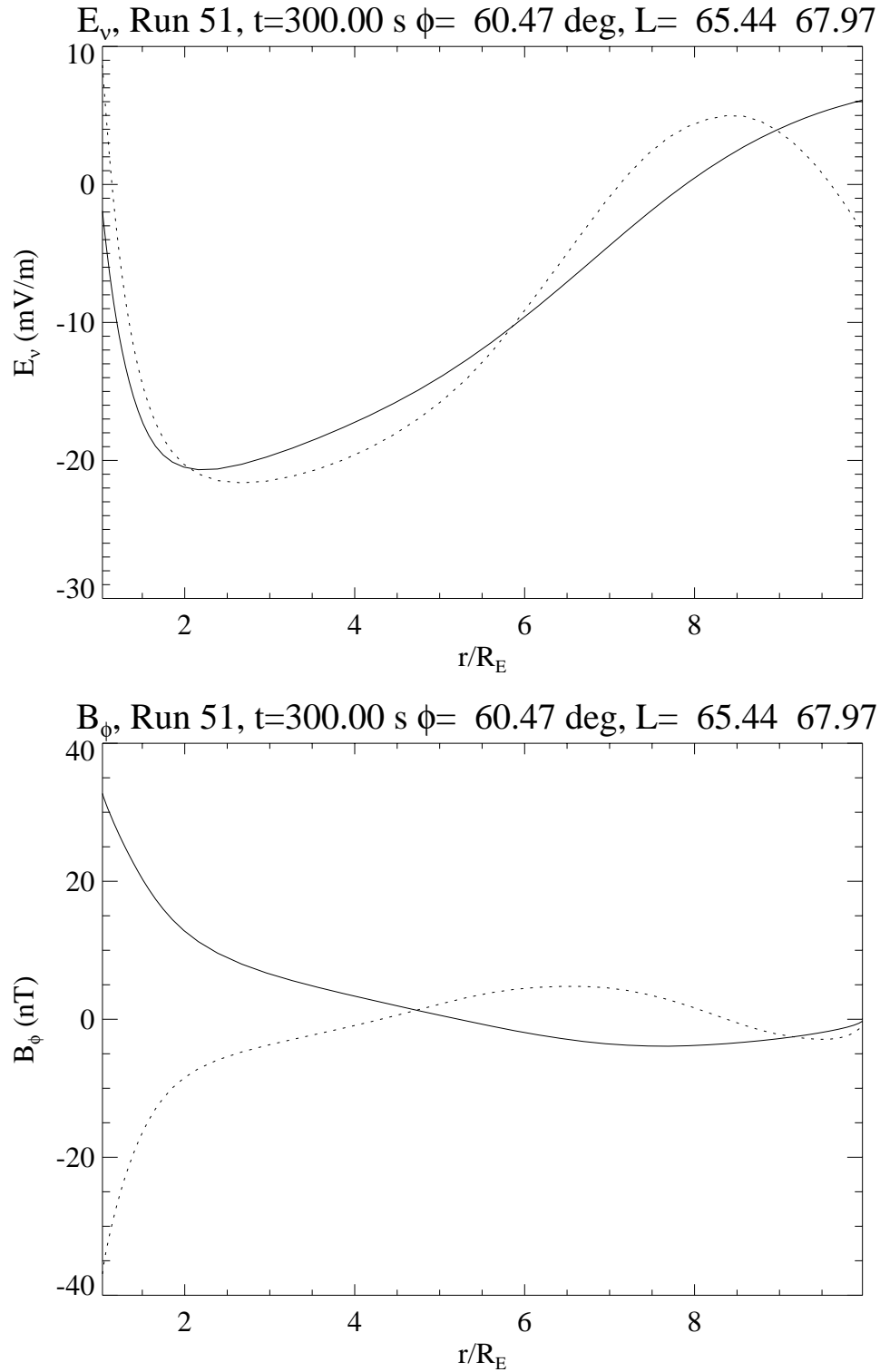


Figure 3. Plots of the (a) poleward perpendicular electric field and (b) eastward magnetic field components at the same time as the plot of Figure 2 at invariant latitudes of  $65.4^\circ$  (solid curves) and  $68.0^\circ$  (dotted curves), indicating 3<sup>rd</sup> and 5<sup>th</sup> harmonic structure, respectively.

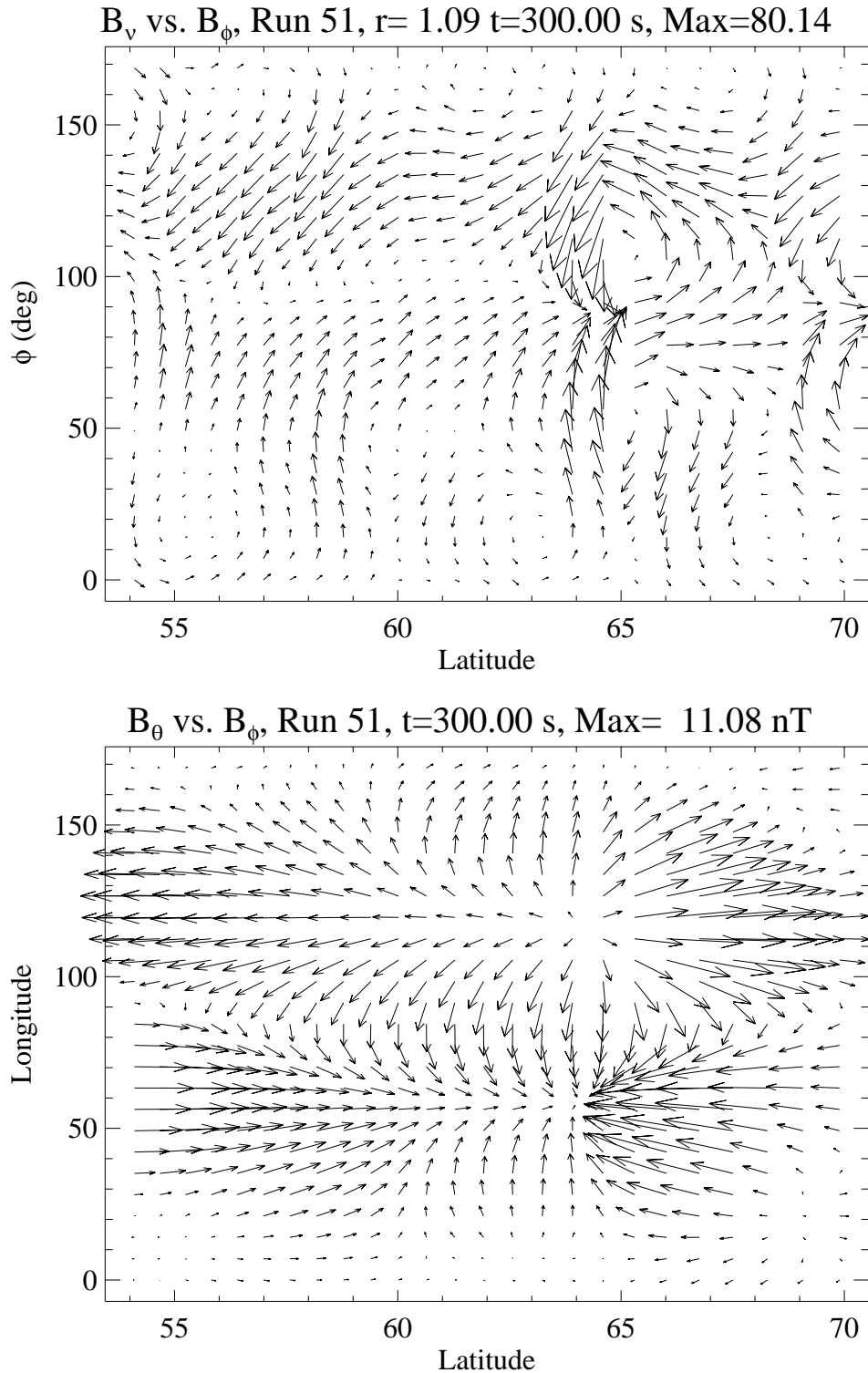


Figure 4. Vector plots of the perpendicular magnetic field at (a) 600 km altitude and (b) the ground at the same time as the plots of Figures 2 and 3. Note the rotation of the magnetic field, the smoothing of the fine scale structure and the general reduction in magnitude from the ionosphere to the ground.

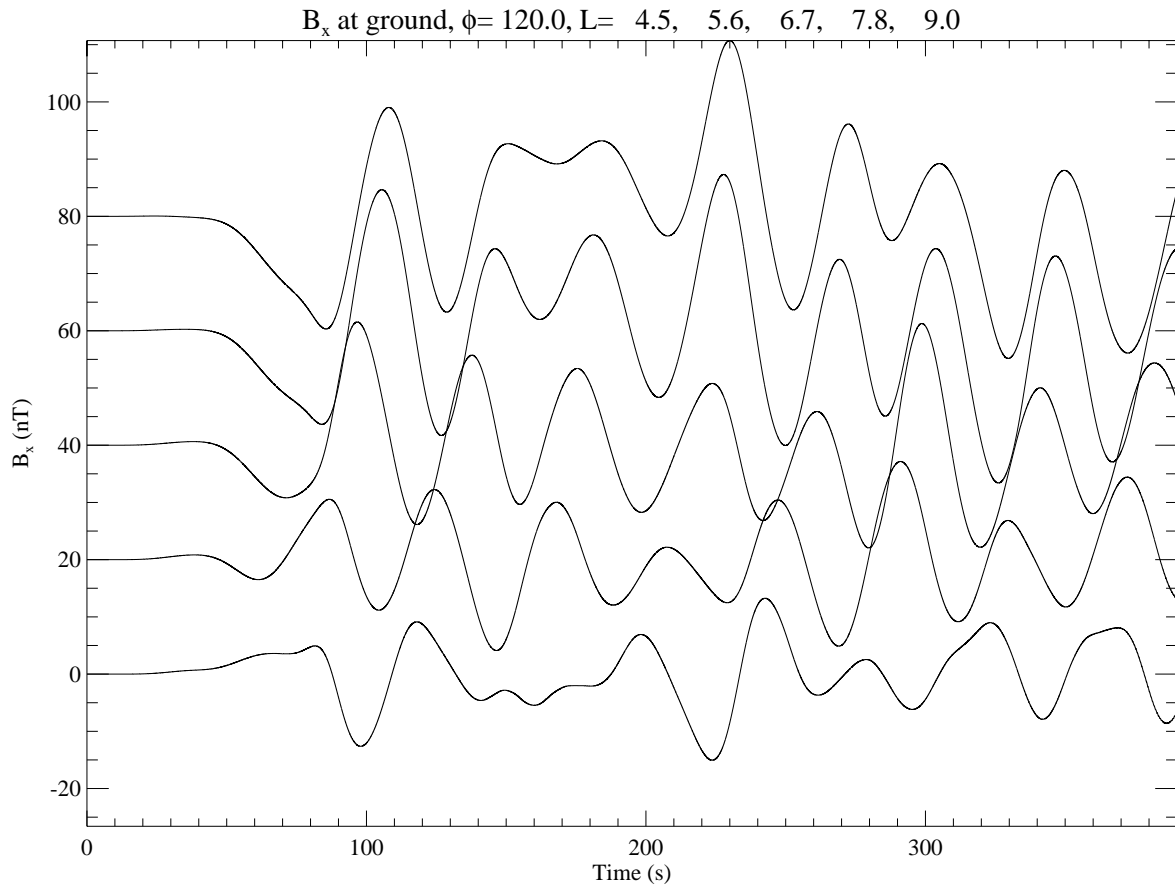


Figure 5. Stacked plots of the time history of the equatorward ground magnetic field at  $120^\circ$  longitude and L values of 4.5, 5.6, 6.7, 7.8, and 9.0, corresponding to latitudes of 61.9, 65.0, 67.3, 69.0 and 70.5 degrees, with the more poleward locations on the top. Note the general poleward phase progressions of the magnetic signals.